POLITECNICO
MILANO 1863

SCUOLA DI INGEGNERIA INDUSTRIALE
E DELL'INFORMAZIONE

EXECUTIVE SUMMARY OF THE THESIS

Comprehensive Analysis of Bevel and Hypoid Gears: Experimental Studies, Simulation Modelling, and In-Depth Evaluation of the FZG Hypoid Test Rig

LAUREA MAGISTRALE IN MECHANICAL ENGINEERING - INGEGNERIA MECCANICA

AUTHOR: UTKU AYRANCILAR, TURAL AGHAYEV

ADVISORS: PROF. CARLO GORLA, PROF. KARSTEN STAHL

CO-ADVISORS: LUCA BONAITI, LORENZ CONSTIEN

ACADEMIC YEAR: 2022-2023

Introduction

Industrial machinery has made incredible strides in the current era of quick advancements in driving technology, which is mainly based on mechanical power transmission. It is crucial to ascertain the mechanical strength properties of components of machines in order to better evaluate their optimal performance. To achieve reliable experimental results for determination of relevant mechanical characteristics, collected outputs have to be sufficiently precise and have negligible variation.

The Back-to-Back Hypoid Test Rig at the Gear Research Center (FZG) at the Institute of Machine Elements of the Technical University of Munich is the subject of this study. This test rig has been developed to experimentally investigate gear failure, providing support to the calculation methods, especially macro pitting failure. The main objective of this study is to determine and evaluate the variables that influence the scatter of experimental results. In detail, in the installation process of gear set, pinion and wheel are accurately installed for proper accumulation of contact pattern on the center of flank surfaces. Following initial load cycles of the fatigue test, this central location can be clearly observed on gear flanks. In contrast, after a large number of cycles, there is a noticeable shifting of contact pattern on the flank surface. Therefore, it is aimed to identify what factors cause the deviation of contact pattern from the center. Detailed formulas and theoretical background are given in the thesis itself. Following the definition of possible influencing variables, the FZG test rig was modeled and various evaluation techniques such as LTCA and statistical techniques were applied.

1. Failure Modes on Bevel & Hypoid Gears

There are several failure modes occurring on gears, such as flank breakage, tooth root breakage, scuffing, rippling, ridging. Pitting is one of the commonly occurring failure types on gears.

Macropitting or pitting is a fatigue failure condition in the active region of tooth flank. Shell-shaped craters are created at the surface when the Hertzian stress is greater than the material strength. These pits continue to increase and finally cause a gear to fail completely as a result of a series of localized failures, as illustrated in Fig 1.1 [6].

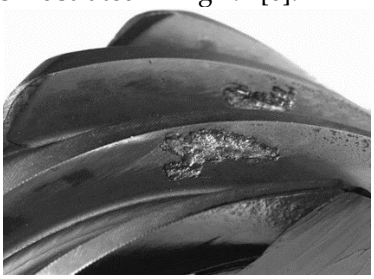

Figure 1.1: Pitting on the Flank Surface [6]

Micropitting is a form of failure that happens when high-stress regions on the surface of a tooth coincide with insufficient lubricating film thickness. As a result, matte gray areas with little cracks and fractures start to form, as shown in Fig 1.2. These fissures eventually grow into tiny craters called "micro" pits, which essentially take material from the surface as a result of wear and tear. In addition to changing the geometry of the tooth flanks and interfering with stress distribution, this process also generates noise, increases dynamic forces, and may have an impact on the capacity for pitting [6].

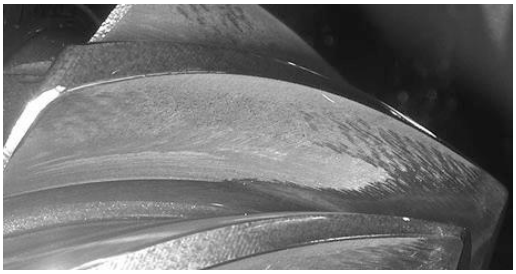

Figure 1.2: Micropitting on the Flank Surface [6]

1.1 Experimental Investigations & Effects of Micropitting

The experimental research carried out by Stahl and at all has made significant progress in comprehension of load capacity calculations for bevel and hypoid gears [4]. This study revealed micro-pitting patterns associated with geometric offsets, shedding light on the complex relationship between micro-pitting, load distribution, and overall gear performance. The study also introduced a novel local calculation method for determining pitting in hypoid and bevel gears. This approach uses loaded tooth contact analysis in accordance with BECAL and related ISO standards for helical gears to account for variables like slip and hypoid effects. By predicting the initiation and dynamics of pitting, it improves the understanding of gear behavior. By incorporating the slip factor for relative sliding and the hypoid factor for lengthwise sliding, designed specifically for hypoid gears, the use of this method for different gear configurations is demonstrated.

Another study investigates micropitting and gray spots in gear mechanisms, relying on Ivan Boiadjiev's doctoral thesis [1] and research at FZG. The "Loss of Drive" failure criterion has been used to evaluate micropitting in gears, but it has limitations, especially for hypoid gears where micropitting and pitting often coexist. By changing the distribution of stress, gray spots have a significant impact on the growth of micropits. They have the ability to either worsen or mitigate micropitting damage. It is difficult to predict micropitting susceptibility only based on initial stress distribution. A more accurate assessment of micropitting susceptibility is provided by the introduction of an extended calculation approach that takes gray spots into account. Under comparable loads, hypoid gears show more rapid micropitting than bevel gears. The results highlight the need for thorough failure criteria that take into account gray spots, shifts in contact pattern, and micropitting, improving gear design and durability evaluations. This study emphasizes the intricate interactions between the development of gray spots, shifting contact patterns, and micropitting damage in gear mechanisms [1, 4]. The outputs of these studies made important contributions and inspirations to the current study on analyzing the effect of micropitting on shifting of contact pattern.

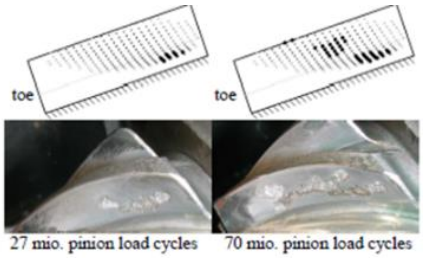

Figure 1.3: Calculated and Experimentally Investigated Results of Pitting [4]

2. FZG Back-to-Back Test Rig for Bevel and Hypoid Gears

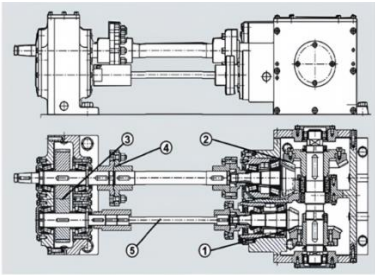

Figure 2.1: FZG back-to-back test rig [3]

This research is centered on the Back-to-Back Hypoid Test Rig at FZG, which ensures experiments in line with the objectives of the study. This rig, which uses torsional shafts, mechanical load clutches, and test gear sets, operates on the closed-cycle principle. The rig is versatile, allowing for a variety of axial offsets and torque values, which makes it perfect for carrying out in-depth research into gear behavior. Especially, this test rig particularly concentrates on experimental investigation of gear failure, with comparison of analytical calculation methods with experimental outputs.

Specifications of the Test Rig [3]:

- **Axial offset**: a = -15, 0, 15, 25, 31.75, 44 mm
- **Max. testing power:** Pmax = 300 kW
- **Speed range:** n1 = 100 - 4800 1/min

The whole systematic procedure of the experimental fatigue tests range from initial assembly of gear set with proper contact pattern adjustment, early short running at low torques, continuous operating of the test cycle under defined torque until the complete failure. These procedures are essential for evaluating elements for pitting and micropitting formation, which are captured in pictures and thorough reports. Overall, the FZG Back-to-Back Hypoid Test Rig offers a necessary platform for conducting in-depth investigations into the behavior of bevel and hypoid gears.

3. Experimental Results

One particular set of experimental results of the performed fatigue test at 400 Nm is presented at Fig 3.1. Photos clearly demonstrate a significant deviation in the location of contact pattern on the pinion flank surface, where considerable micropitting emerges after a certain number of load cycles, particularly toward the heel of the tooth. On the other hand, the contact pattern stays nearly in the center of the flank surface on the wheel flank, where micropitting is substantially less noticeable. Therefore, this evidence strongly finds that the occurrence of micropitting is the main factor influencing the shift of the contact pattern on the flank surface.

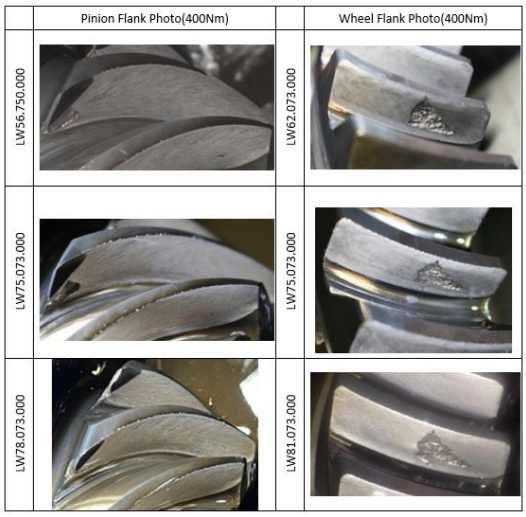

Figure 3.1: Some Critical Exp. Results

4. Simulation Modelling of FZG Hypoid Test Rig & LTCA

Despite the clear confirmation regarding the significant impact of micropitting on the dispersion of experimental results, there might be still some other variables which also lead to such deviation. Basically, two factors are defined to be analyzed, input load, with its fluctuation, and preloading on pinion shaft bearings.

This section explores the use of the SMT Masta Program for modeling and simulation of the FZG Test Rig, in order to identify the dominance of those two factors on the scatter of experimental results. The entire analysis procedure is graphically explained below:

Figure 4.1 Graphical Description of the Analysis of Influences of Factors

SMT Masta is a flexible program renowned for its abilities to carry out a variety of analyses, including NVH, deflection, durability, and FE. It was used to model the FZG Test Rig, allowing simulations at various combinations of input load and preloading on pinion shaft bearings.

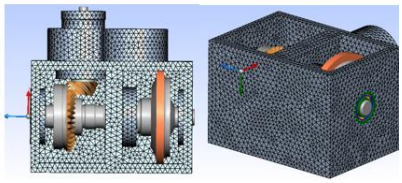

Figure 4.2: MASTA Model of the Test Rig

Spiral bevel gears can be designed, optimized, and produced with using KIMoS. In current study, KIMoS was used to create the main geometrical dimensions of pinion and wheel. The parameters are given below.

G31.75	sym.	Bevel stage		unit
		Pinion	Gear	
Number of teeth	z	9	34	-
Shaft angle	Σ	90		°
Axial offset	a	31.75		mm
Normal module (tooth center)	m_{mn}	3.988		mm
Normal module	m_{mn}	3.988	3.988	mm
Mean helix angle	β_m	-44.932	20.975	°
Reference cone angle	δ	24.822	63.155	°
Tip angle	δ_a	24.822	63.155	°
Root angle	δ_f	24.822	63.155	°
Normal pressure angle traction	α_{nZ}	17.393		°
Normal pressure angle thrust	α_{nS}	22.318		°
Spiral angle pitch direction		left	right	-
Face width	b	31.132	26	mm
Mean reference cone distance	R_m	60.387	81.381	mm
Outer tooth depth	h_e	9.071	9.071	mm
Addendum modification coeff.	x_{hm}	0.455	-0.455	-
Tooth thickness modification factor	x_{sm}	0.039	-0.058	-
Mean normal chordal thickness (KIMOS)	Snm	7.911	4.522	mm
Mean normal circular thickness (ISO 23509)	s_{mn}	7.889	4.49	mm
Mean normal chordal thickness (ISO 23509)	s_{mnc}	7.881	4.49	mm
Mean transvers circular thickness (ISO 23509)	s_{mt}	11.144	4.809	mm
Mean transverse chordal thickness (ISO 23509)	s_{mtc}	11.07	4.809	mm

Table 4.1: G31.75 Gear Geometrical Dimensions

4.1 Results of the Test Rig Simulation Model

To analyze the test rig behavior under various conditions, two selected factors are chosen at a specified range of values and the simulation was repeated for all combinations of those values. The input torque was changed between 100 Nm and 700 Nm, while the preloading on pinion shaft bearings were ranged from 0 to 200 µm. Noting that, for all cases, both bearings on the pinion shaft were preloaded in the same amount.

The simulation outputs were achieved in terms of gear set misalignments. At SMT Masta, misalignments are identified with four components: axial displacement of wheel and pinion, radial displacement of wheel and shaft angle. The variation trend of all misalignment components with respect to preloading on pinion shaft bearings, under several input torques are illustrated below:

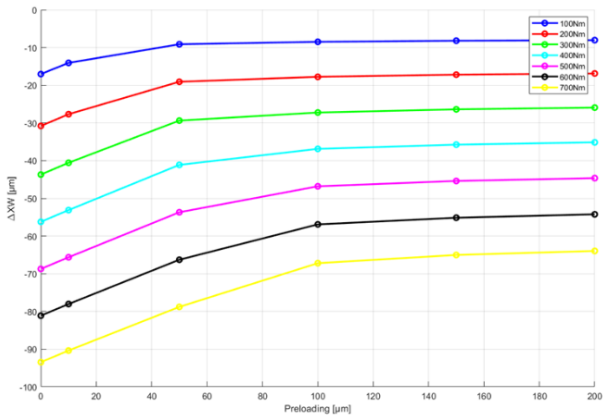

Figure 4.3: Variation of wheel axial displacement with respect to different preloading values on pinion shaft bearings, under varying input torque quantities

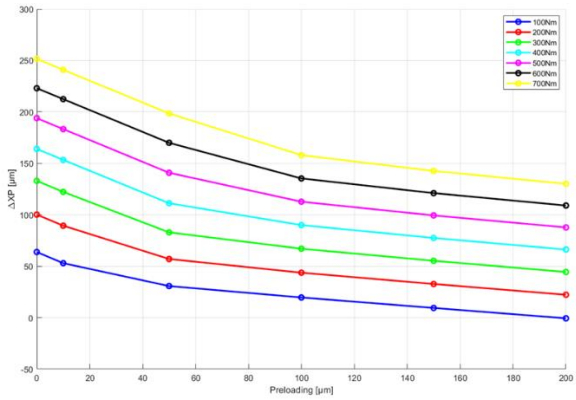

Figure 4.4: Variation of pinion axial displacement with respect to different preloading values on pinion shaft bearings, under varying input torque quantities

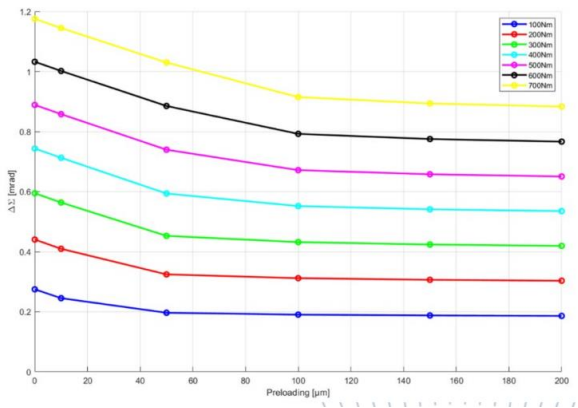

Figure 4.5: Variation of shaft angle with respect to different preloading values on pinion shaft bearings, under varying input torque quantities

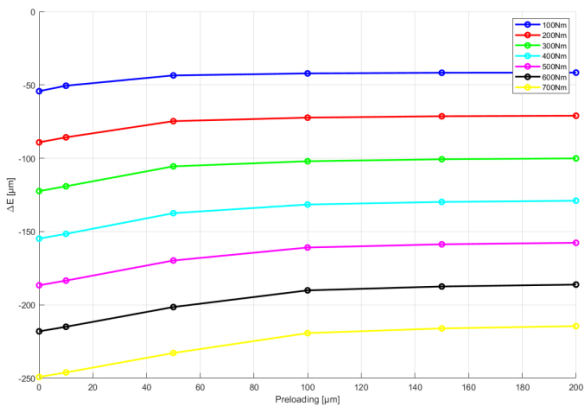

Figure 4.6: Variation of wheel radial displacement with respect to different preloading values on pinion shaft bearings, under varying input torque quantities

It is clear from the simulation results that absolute values of all four of the misalignment components rise with increasing input torque. Indeed, higher torque levels result in higher axial and radial deflections of the wheel and pinion. On the other hand, an increase in the preload on the pinion shaft bearings contributes to increased rigidity of gear set, therefore lower misalignments. It is noteworthy that the misalignment values do not decrease as sharply as initially observed beyond a certain threshold of bearing preload. This implies that beyond a certain point, excessive bearing preload does not significantly contribute to increasing the rigidity of the contact pattern on gear flanks. These misalignment outputs were imported to BECAL software for LTCA analyses in the subsequent step. Meanwhile, for the validation of current simulation outputs, the further results produced at FZG studies around a decade ago, were referred. As seen in Fig 4.7, which compares those reference results and a recent simulation output set at a certain preloading on pinion shaft bearings, the variation pattern of misalignment with respect to input torques is very comparable for both cases (linear rise). These highly similar outcomes further prove that current simulation results have sufficient reliability to be applied in LTCA analyses.

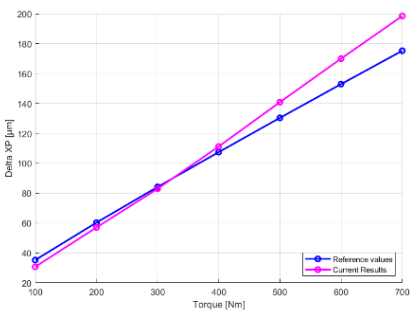

Figure 4.7: Comparison between reference results and current simulation results

4.2 LTCA Results

Subsequently, LTCA analyses were conducted at BECAL software by importing misalignment outputs. Through these analyses, the distribution of flank pressure on flank surface (contact pattern) with its maximum value and corresponding location, were achieved for several preloading values and specifically for 400Nm. Analyzing the variation of the maximum flank pressure with respect to preloading on pinion shaft bearings, on Fig 4.8, it can be identified that smaller preload values result in a significant reduction in maximum flank pressure, which is followed by a gradual convergence as preload values rise.

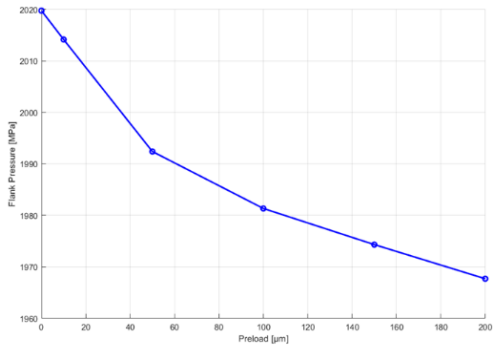

Figure 4.8: The maximum flank pressure variation with respect to preloading on pinion shaft bearings

However, the highest pressures on the flank surface for various preload values do not differ significantly, as 200 µm change of preloading contributes to only 52 MPa change in maximum flank pressure. Compared to the average value of all maximum flank pressures, this change only accounts for about 2%. Moreover, there is no significant shift in the contact pattern location when observing the distribution of the contact pattern on the flank surface under various preload conditions. This suggests that changes in preload on pinion shaft bearings do not exert a dominant effect on the shift of the contact pattern on the flank surface.

The impact of minor torque variations on the contact pattern was also examined as input torque slightly fluctuates during the entire testing. With torque values of 390 Nm and 410 Nm, which are variations of about 10 Nm from the original 400 Nm, LTCA analyses were conducted. The findings are displayed in Figure 4.9 and show that, for all preload values, a 10 Nm torque variation corresponds to a small 13 MPa flank pressure variation. This variation is mere 0.6% of the average value of the maximum flank pressures. Furthermore, contact patterns for these three

torques under the same preloading do not differ reasonably, in case of any preloading on pinion shaft bearings. As a result, slight torque variations have only a little effect on the shift of the contact pattern and do not play a substantial role on the not accumulation of the contact pattern in the middle of the flank surface.

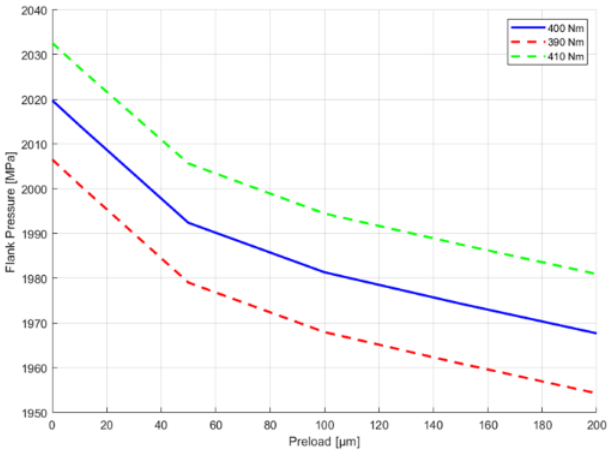

Figure 4.9: Flank pressure variation with respect to preloading on pinion shaft bearings for different torque values

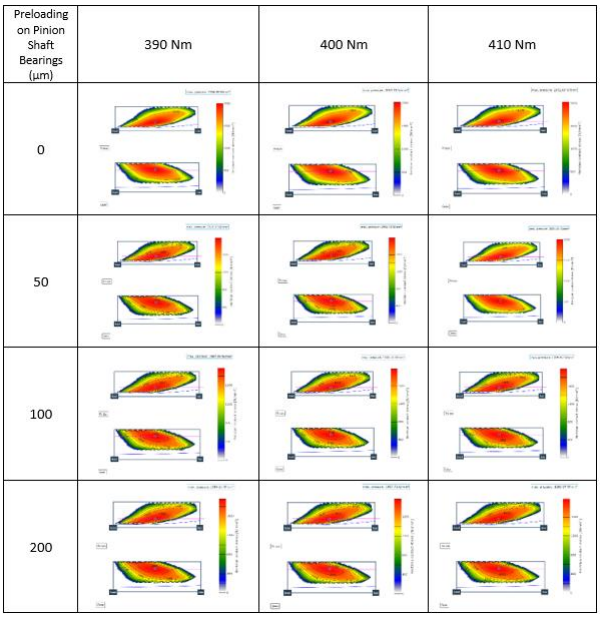

Figure 4.10: LTCA Test Results from BECAL for Different Preloading on Pinion Shaft Bearings (µm)

5. Sensitivity Analysis of the Torque Measurement System of the FZG Hypoid Test Rig

Figure 5.1: The Calibration Setup Installed on the FZG Hypoid Test Rig

Despite the consideration of input torque and its minor variations as not primary contributor on the dispersion of experimental results, input loading can still be a concerning issue. To elaborate, it is necessary to confirm whether there is a sufficient alignment between applied torque to the test cycle by suitable tools and displayed torque reading on the measurement device. Therefore, this section aims to carry out a relevant sensitivity analysis on the torque measurement system in order to check its accuracy.

5.1 Calibration of the Torque Measuring System on the FZG Hypoid Test Rig

Following DIN 51309 [2] guidelines, the torque measurement system on the Back-to-Back Hypoid Test Rig was calibrated using a lever-mass system. In order to produce discrete torque values, weights added sequentially, while display readings in terms of voltage were recorded. Generally, calibration setup includes a fuser unit, calibration lever, hanger, and nine additional calibration weights. According to DIN 51309 [2] standards, the calibration test has to be repeated at a total of four positions of the test rig shaft. Due to geometrical configuration of teeth on test rig coupling and those of fuser unit, test rig was every time rotated 180 degrees to achieve the new position. Basic load spectrum (three fully preloadings and upward-downward-upward discrete load series) was applied for loading at position 1, whereas reduced load spectrum (one fully preloading and upward-downward discrete loading series) was applied for other positions.

After the whole data collection process, all values are properly averaged in terms of position and upward-downward manner, in order to achieve single voltage value for each discrete torque. Furthermore, relevant techniques of DIN 51309 was applied for calculating reproducibility, zero-point deviation, interpolation deviation values. Based on digit fluctuation, the system resolution was determined to be "0.001".

Afterwards, mean and standard deviation values of calibration weights and moment arm, as shown in Table 5.1, were inputted to GUM-Workbench [5] in order to obtain each relative standard deviation determined by the influence of corresponding calibration torque with type of distribution, as illustrated in Table 5.2.

Physical Quantity	Average Value	Standard Deviation
m_lever	1725 kg	0.05 kg
m_hanger	4.4 kg	0.05 kg
m 4	5.2 kg	0.05 kg
m 5	6.8 kg	0.05 kg
m 6	8.4 kg	0.05kg
m 7	9.8 kg	0.05 kg
m 8	11.4 kg	0.05 kg
m 9	12.8 kg	0.05 kg
m 10	14.4 kg	0.05 kg
m 11	15.8 kg	0.05 kg
m 12	17.2 kg	0.05 kg
L	0.5 m	0.005 m
g	9.807595 m/s²	698e-06 m/s²

Table 5.1: Standard deviations of physical quantities used to calculate calibration torques

Torque	Value	Relative Standard Deviation	k factor	Type of Distribution	w_{KB} (%)
M_0	0 Nm	0	2.00	95% (Normal)	0
M_1	8.46 Nm	3.1 %	1.77	%95 (Trapesoidal, Form factor = 0.5)	1.7514
M_2	30.04 Nm	1.6 %	2.00	95% (Normal)	0.8
M_3	55.54 Nm	1.3 %	2.00	95% (Normal)	0.65
M_4	88.90 Nm	1.1 %	1.85	%95 (Trapesoidal, Form factor = 0.3)	0.5946
M_5	130.1 Nm	1.1 %	1.77	%95 (Trapesoidal, Form factor = 0.5)	0.6215
M_6	178.1 Nm	1.0 %	1.77	%95 (Trapesoidal, Form factor = 0.5)	0.565
M_7	234.0 Nm	1.0 %	1.77	%95 (Trapesoidal, Form factor = 0.5)	0.565
M_8	296.8 Nm	0.98 %	1.69	%95 (Trapesoidal, Form factor = 0.7)	0.5799
M_9	367.4 Nm	0.97 %	1.69	%95 (Trapesoidal, Form factor = 0.7)	0.574
M_{10}	444.9 Nm	0.97 %	1.69	%95 (Trapesoidal, Form factor = 0.7)	0.574
M_{11}	529.2 Nm	0.97 %	1.69	%95 (Trapesoidal, Form factor = 0.7)	0.574

Table 5.2: Calibration torque values with relative standard deviations

Finally, after calculating all relative standard deviation components determined by the influences of all other elements, the relevant equation was used to combine these values, for calculating relative extended uncertainty for each torque level.

Display [V]	$W_{abs}[V]$	M_K [Nm]	$\pm\Delta M_K$ [Nm]	$W(M_K)$
0	0	0	0	0
0.064875	± 0.010397	8.46	1.36	0.16025
0.23662	± 0.011152	30.04	1.42	0.047128
0.43688	± 0.011919	55.54	1.52	0.027282
0.70112	± 0.012606	88.90	1.60	0.017979
1.0186	± 0.017296	130.10	2.21	0.01698
1.3995	± 0.020958	178.10	2.67	0.014975
1.835	± 0.022868	234.00	2.92	0.012462
2.3306	± 0.03242	296.80	4.13	0.01391
2.8814	± 0.035765	367.40	4.56	0.012413
3.4816	± 0.056143	444.90	7.17	0.016125
4.116	± 0.14686	529.20	18.89	0.03568

Table 5.3: Relative extended uncertainty and Absolute extended uncertainties

Considering results at Table 5.3, it can be noticed that there is a substantially smaller relative extended uncertainties compared to corresponding calibration torques. Only for M_2, the value is reasonably greater than other levels. It can be explained by significant interpolation deviation, as data points follow polynominal rather than linear behaviour at low torque values. For nearly all torque levels, minor torque variations do not even exceed 10 Nm. As specified in 4.2, the ±10 Nm fluctuation has a negligible effect on the maximum flank pressure and contact pattern shifting. As a result, torque uncertainties do not have a substantial effect on scatter of test results and the torque measurement system can be certainly considered sufficiently accurate to precisely measure applied torque during testing.

6. Conclusion

Here, it has been studied what causes the scatter of the experimental test results at the Back-to-Back Hypoid Test Rig at the Gear Research Center (FZG). In particular, it was examined to identify the sources of occurrence of pitting on shifted position on gear flanks, despite initial arrangement of contact pattern on the center of flank surface. Together with the related literature, it was found by experimental testing results that the existence of micropitting on flank surfaces can considerably lead to the shifting of contact pattern. Afterwards, other possible variables that might also influence on the deviation of experimental results were analyzed, such as input torque, its minor fluctuations, preloading on pinion shaft bearings and accuracy of torque measurement system. According to the findings from appropriate analysis methods, it was determined that none of these variables has a significant effect on the deviation of contact pattern. As a result, the micropitting was identified as the dominant influencing factor on the scatter of the experimental results.

References

[1] Boiadjiev, I. (2019). Schadensentwicklung und tragfähigkeit carbonitrierter Kegelradverzahnungen Untersuchung der tragfähigkeit von carbonitrierten kegelrad- und Hypoidverzahnungen (thesis).

[2] DIN 51309. (2005).

[3] FZG Website. Startseite. (2023). https://www.mec.ed.tum.de/fzg/startseite/

[4] Höhn, B. R., Stahl, K., & Wirth, C. (2011). New calculation method for the load capacity of bevel and hypoid gears based on loaded tooth contact analysis. Applied Mechanics and Materials.

[5] JCGM 100.2008. (2008). Guide to the expression of uncertainty in measurement - JCGM 100:2008 (GUM)

[6] Klingelnberg, J. (2016). Bevel Gear Fundamentals and Applications. Springer.